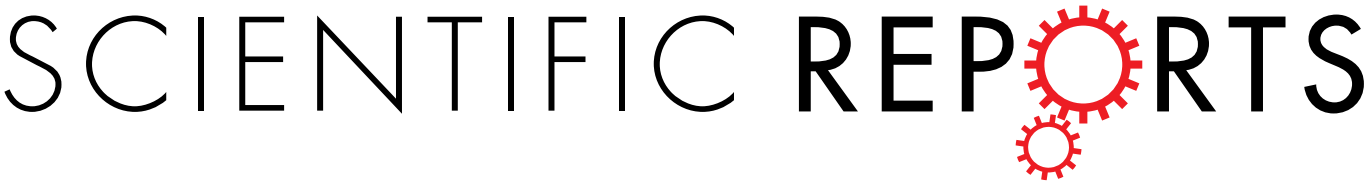

OPEN

Three dimensional Graphene aerogels as binder-less, freestanding, elastic and high-performance electrodes for lithium-ion batteries

Received: 08 February 2016
Accepted: 17 May 2016
Published: 06 June 2016

Zhihang Chen[1], Hua Li[1,2], Ran Tian[1], Huanan Duan[1], Yiping Guo[1], Yujie Chen[1], Jie Zhou[1], Chunmei Zhang[1], Roberto DUGNANI[3] & Hezhou Liu[1,2]

In this work it is shown how porous graphene aerogels fabricated by an eco-friendly and simple technological process, could be used as electrodes in lithium- ion batteries. The proposed graphene framework exhibited excellent performance including high reversible capacities, superior cycling stability and rate capability. A significantly lower temperature (75 °C) than the one currently utilized in battery manufacturing was utilized for self-assembly hence providing potential significant savings to the industrial production. After annealing at 600 °C, the formation of Sn-C-O bonds between the SnO_2 nanoparticles and the reduced graphene sheets will initiate synergistic effect and improve the electrochemical performance. The XPS patterns revealed the formation of Sn-C-O bonds. Both SEM and TEM imaging of the electrode material showed that the three dimensional network of graphene aerogels and the SnO_2 particles were distributed homogeneously on graphene sheets. Finally, the electrochemical properties of the samples as active anode materials for lithium-ion batteries were tested and examined by constant current charge–discharge cycling and the finding fully described in this manuscript.

Because of the high specific energy, long cycle life and environmental protection, LIBs have become the main supporting power for all kinds of advanced portable electronic products. With the development of new electrode materials and technology innovations, LIBs which have high charge-discharge rate and specific capacity, have shown great advantages in the electronic field[1–4]. It has been reported that several kinds of nanostructured, transition-metal oxides[5] such as SnO_2 nano-particles can improve the performance of rechargeable LIBs[6]. Single layer, two dimensional graphene has a significantly larger theoretical capacity than graphite and is favorable to lithium ion transport resulting in improving the overall performance of LIBs. But, it is well-known that when graphene is used as lithium-ion batteries electrode materials, the powerful π-π stacking interactions and Van Der Waals forces make graphene sheets easily aggregate into powders or films which in turn induce higher resistance for Li^+ ion diffusion and decrease surface area significantly[7,8]. Graphene aerogels (GA) display three dimensional porous frameworks, large specific surface area, rapid ion-diffusion characteristics, excellent mechanical strength as well as multidimensional continuous electron-transport pathways and have been fabricated and designed for energy storage and conversion, adsorbents for environmental remediation and catalysis[9,10]. Moreover, nano-porous structures could provide additional channels for Li^+ ions and electrons transmission during the lithiation and delithiation processes[11,12]. Three dimensional graphene could offer space for ions expansion and electrolyte storage[8,13–15]. In order to take advantage of these features displayed by graphene aerogels, scientists have recently paid increasing attention to the combination of graphene aerogels and LIBs.

[1]State Key Laboratory of Metal Matrix Composites, School of Materials Science and Engineering, Shanghai Jiaotong University, China. [2]Collaborative Innovation Center for Advanced Ship and deep-Sea Exploration, Shanghai Jiao Tong University, China. [3]University of Michigan- Shanghai Jiaotong University Joint Institute, China. Correspondence and requests for materials should be addressed to H.Li (email: lih@sjtu.edu.cn) or H.Liu (email: hzhliu@sjtu.edu.cn)

Currently, most studies describe graphene hydrogels preparation by hydrothermal method[5,16,17], which transfers the mixture solution into a poly (tetrafluoroethylene) (Teflon)-lined autoclave (50 mL) heated at 160 to 200 °C for 5 to 24 hours. Since such preparation method requires relatively high temperature it clearly is not viable for industrial production. Moreover, it has been a recent practice for graphene aerogels to be grinded into powder and mixed with several kinds of conductive agents and binders when using graphene as the cathode material for lithium-ion batteries[18,19]. Jun Zhang[20] fabricated SnO_2/graphene composites used as anode material by a hydrothermal method with a process heating to 200 °C for 24 h. What is more, the composites were grinded into powder and then mixed with acetylene carbon black (15 wt%) and polyvinylidene fluoride(10 wt%) in N-methyl-2-pyrrolidone (NMP). Lastly, vacuum treatment for 12 h was required to prepare working electrods. Nonetheless, this strategy could not take full advantage of the virtues of GA as clearly the grinding process disrupts the natural GA's 3D framework. Additionally, conductive agents and binders are indispensable in this type of manufacturing hence increasing the weight of the batteries and complicating the manufacturing process. Thus, such method not only has a lengthy manufacturing process, but also cannot take fully advantage of the aerogel as a three dimensional conductive network.

Herein, we proposed and developed a simple yet novel strategy to fabricate porous SnO_2-reduced graphene aerogels which have the merits of excellent cycling performance, environmental friendliness, and simple manufacturing process. In the synthesis process for graphene hydrogels, graphene oxide was reduced in a simple mold at low temperature (75 °C). Moreover, Sn-C-O bonds between SnO_2 nanoparticles and GS were formed after annealing at 600 °C, which will initiate synergistic effect as well as improve the electrochemical performance. Graphene aerogels could then be used as LIBs electrode materials without any further processing or binder addition. Such freestanding and binder-less 3-D graphene with a remarkably high specific surface area and due to the porous structure and an excellent conductivity[21] was fabricated with a molding technology, which could simplify the preparation for LIBs electrodes as well as avoid adding superfluous material. These auxiliary additives and binder would result in a "dead surface" and a larger resistance[22,23]. In this strategy, GA was fully used which would reduce the weight of the batteries and was low-cost. Moreover, these 3D graphene structure could alleviate irreversible restacking and agglomeration caused by the powerful π-πstacking interactions and Van Der Waals forces, as well as promote the transportation of electrolytes within the electrodes[21,24].

Results

Three dimensional and cylindrical SnO_2/graphene aerogels which could be used in LIBs without any conductive agent and binder was successfully prepared and characterized in this work. In the proposed manufacturing method, the significantly lower SnO_2/graphene self-assembly temperature of 75 °C (reduced from typical values of 180 °C or more than 180 °C[25,26]) is expected to bring significant savings to industrial production. According to the SEM and TEM imaging, a uniform set of SnO_2 nanoparticles with diameter in the range of 4~10 nm were firmly anchored on the graphene sheets likely resulting in improved electrochemical properties of the material. Such a three-dimensional porous framework was shown to effectively eliminate SnO_2 aggregation, provide room for particles expansion and facilitate lithium ions and electrons transport. Also, the synergistic effect between flexible graphene layers and nano-sized SnO_2 improve the capacity and cyclic stability. The described superior properties are believed to result mainly form the high specific surface area and the excellent conductivity of the electrode material.

Discussion

Homogenous SnO_2 dispersion was prepared through a hydrothermal method[27–29]. SnO_2-GA three dimensional porous aerogels were fabricated by a hypothermal self-assembly strategy which we believe to be more suitable for industrial production.

SnO_2 particles with positive surface charge have a tendency to attract negatively charged oxygen-containing functional groups on graphene oxide[11]. Thus, SnO_2 nanoparticles with a diameter of 4~10 nm would adhere to the surface of graphene sheets (GS) tightly as a result of electrostatic attraction[30,31]. Moreover, because of the strong electrostatic attraction, SnO_2 particles will remain anchored on the surface of graphene sheets after sonication and stirring. The dark brown color of the SnO_2-GO dispersion suggested that the SnO_2 nanoparticles were adhering directly onto the graphene sheets. Subsequently, L-ascorbic acid was used as reducing agent to transform *in situ* Graphene Oxide (GO) into reduced GO (rGO)[8]. As a result of the decrease of oxygen-containing groups on the surface of GS and driven by π-π stacking interactions, GO anchored with SnO_2 particles was reduced to GS and self-assembled into a 3D hydrogel. Such reaction would result in the increase and enlargement of delocalized π-bond's conjugative effect[32]. After these reactions, various oxygen containing functional groups were found to be left on the surface of rGO nano-sheets. Since the SnO_2 nanoparticles had polar surfaces, they interacted with functional groups via hydrogen bonding[6,27,30]. Such hydrogen bonding could transform into oxygen bridges between SnO_2 and rGO by forming Sn-O-C bonds after annealing at 600 °C. Moreover, such bridges would stabilize the SnO_2 nanoparticles on the graphene surface, moreover, facilitate the electron, transfer and improve the electrode stability[4,33] and initiate synergistic effect.

It is known that graphene aerogels have excellent conductivity and mechanical strength which suggests that graphene aerogels could be directly used as electrodes without any additional additives[13,34]. The synthesis procedure of SnO_2/Graphene hydrogels is schematically shown in Fig. 1 by hypothermal hybridization. After freeze-drying, graphene aerogels where obtained in shape and sizes comparable the ones obtained by GHs.

The morphologies of SnO_2-GA were characterized both by scanning electron microscopy (SEM) and transmission electron microscopy (TEM). Figure 2(A) shows an SEM image of the laminar graphene aerogels, which displays an interconnected and porous morphology. The size of the pores ranged from 10 μm to 50 μm with the pore walls consisting of thin layers of graphene sheets formed during the self-assembly of graphene. The TEM

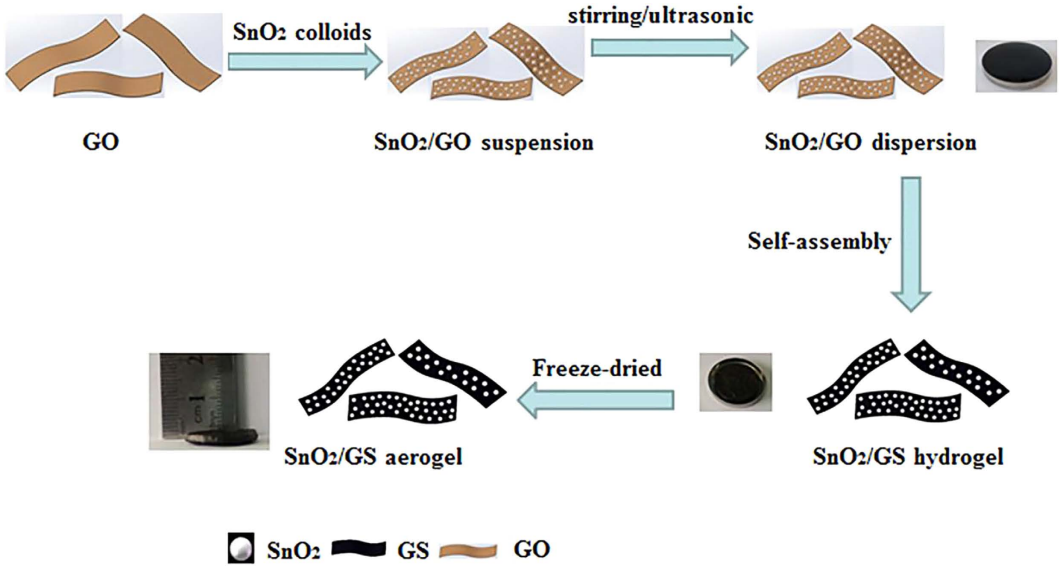

Figure 1. Schematic synthesis procedure of the preparation of the SnO_2-GA and SnO_2-rGA.

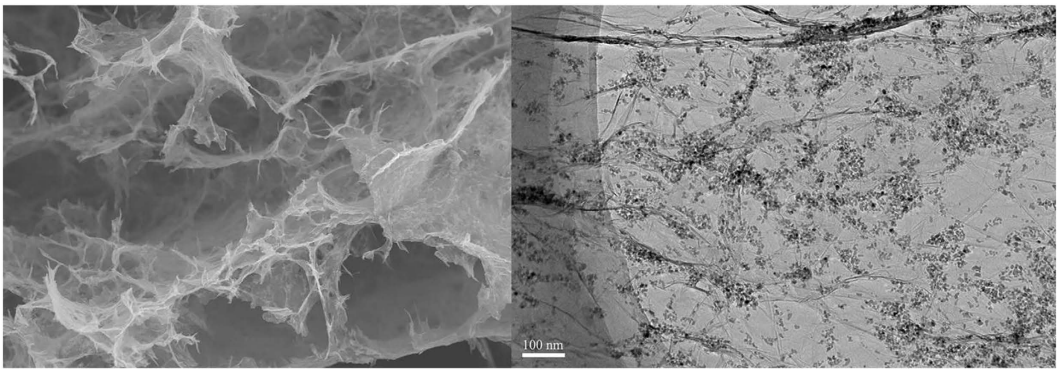

Figure 2. (**A**) SEM image of SnO_2-GO composite at low magnification with a flake. (**B**) TEM image of SnO_2-GO composite. (**C**) TEM image of SnO_2-GO composite after one charge/discharge cycle.

images (Fig. 2(B)) show that the size of SnO_2 nanoparticles were approximately in the range of 4 nm to 10 nm, moreover, the nanoparticles appeared to anchor on the GS firmly and homogeneously.

Figure S(1) shows the Raman spectra of SnO_2-rGA and SnO_2-GA. For SnO_2-rGA; the two prominent peaks at ~1339 cm^{-1} and ~1576.5 cm^{-1} corresponded to D and G bands, respectively. For SnO_2-GA, the G-band was around 1338 cm^{-1} and the D bands was around 1577 cm^{-1}. The intensity ration of the D to G peak (I_D/I_G) increased from 1.199 to 1.283, which could be explained by the size decrease of the sp^2 domain and confirmed the reduction of graphene oxide after heat treatment[35,36].

X-ray photoelectron spectroscopy (XPS) was carried out to confirm the surface chemical state and the chemical elements in the framework after annealing. According to the high-resolution scan spectrum (Fig. 3(A)), it was found that the sample only contained C, O and Sn. The peaks of C1s, O1s and Sn3d were at 284.6, 530.6, and 486.6 eV[30,37]. Figure 3(B) revealed the XPS spectrum of Sn3d. There were two peaks located at 487.2 and 495.6 eV which corresponded to $Sn3d_{5/2}$and $Sn3d_{3/2}$. The peak at 487.2 eV of $Sn3d_{5/2}$ belonged to Sn^{4+} in SnO_2[7]. This peak confirmed the presence of SnO_2 on the surface of graphene layers. The peak of O1s was shown in Fig. 3(C). There were three predominant peaks located at 531.1, 532.2 and 533.4 eV, which corresponded to Sn-O and/or C = O bonds, Sn-C-O bonds, and C-OH and/or C-O-C groups (hydroxyl and/or epoxy)[38], respectively. The Sn-C-O bonds formed after annealing treatment revealed the widespread connection between graphene layers and the SnO_2 nanoparticles, which could initiate synergistic effect and improve the electrochemical properties[38,39]. Before annealing at 600 °C, the connection between SnO_2 nanoparticles and GS was physisorption. Without any chemical bonds, the interaction between SnO_2 nanoparticles and GS was Van der Waals force and hydrogen bond, the SnO_2 nanoparticles may separate form GS during Li^+ insertion and extraction, resulting in the attenuation of capacity during charge/discharge cycling. After annealing at 600 °C, the hydrogen bonds transform into oxygen bridges and form Sn-C-O bonds, which would strongly anchor the SnO_2 nanoparticles and initiate synergistic effect. The synergistic effect between GS and SnO_2 nanoparticles was larger than the contribution of all

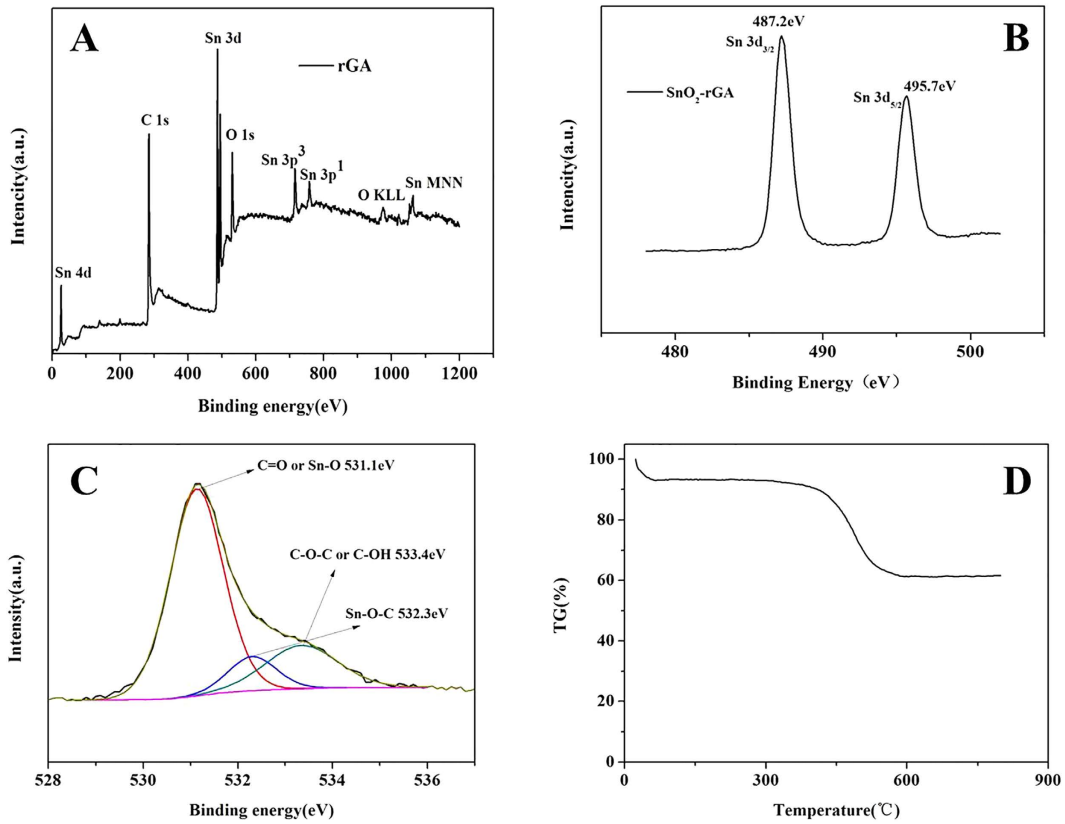

Figure 3. (**A**) High resolution XPS spectra of SnO_2-rGA; (**B**) Sn 3d XPS spectrum of SnO_2-rGA; (**C**) O1s XPS spectrum of SnO_2-rGA; (**D**) The TGA between 20 °C and 800 °C.

constitutive components[40]. Moreover, such bridges facilitate the transport and the reversible lithiation and delithiation, leading to a superior cycling stability and rate capability[41].

The amount of SnO_2 anchored on the graphene sheets' surface in the nano-composites was tested by thermogravimetric analysis (TGA) from 25 °C to 800 °C with a heating rate of 5 °C min^{-1} (Fig. 3(D)). A severe weight loss was noted between 400 °C and 550 °C due to the decomposition of the graphene layers. The weight ratio of GA was calculated to be 66.02%.

The specific resistance and the square resistance of SnO_2-GA was measured to be 650 mΩ cm^{-1} and 7000 mΩ cm^{-1} through a four probes method, suggesting the GA could transport electrons quickly as a result of the three dimensional electrically conducting framework. The excellent measured conductivity is expected to result in a superior electrochemical performance of the electrode.

To evaluate the electrochemical properties of SnO_2-GA systematically, galvanostatic discharge-charge (lithium insertion-lithium extraction) measurements with current density of 200 mA g^{-1} with voltage between 0.01 and 3 V, were carried out. It was noteworthy that the specific capacities were calculated on the basis of the weight of the active nanocomposites materials. Figure 4(A) shows the long cycle performance of SnO_2-GA using charge-discharge repetition at a current density of 100 mA g^{-1}, the typical charge-discharge profiles of SnO_2-GA in the 1st, 2nd, 10th, 50th, 100th and 200th cycles are shown in Fig. 4(B). In the first cycle, SnO_2-GA displays a discharging capacity of 1295.2 mAh g^{-1} and a reversible lithium de-intercalation charging capacity of 857.9 mAh g^{-1} with coulombic efficiency of 66.2%. In the second cycle, the reversible discharge capacity of SnO_2-GA was found to be 866.6 mAh g^{-1}. Subsequently the value decreases to 783.5 mAh g^{-1} in the 31th cycle and then increased to 867.3 mAh g^{-1} in the 99th cycle. Moreover, the coulombic efficiency was found to be higher than 96.5% after the 3rd cycle. Because the graphene structure was porous and elastic, when graphene nanostructure was compressed and used as electrodes, the porous structure prevented substantial shrinkage. Furthermore, the structure subsequently inflated during the charge/discharge cycles[8,29,42]. The contact was improved along with the inflation, which could result in the increase of charge/discharge capacity. The rate characteristic of the SnO_2-GA at different current densities of 100 mA g^{-1}, 200 mA g^{-1}, 500 mA g^{-1},1500 mA g^{-1}, 3000 mA g^{-1} are illustrated in Fig. 4(C). There was almost no decrease of reversible capacity at a low density of 100 mA g^{-1}. Furthermore, the capacity not only did not decrease, but even increased at higher current density of 200 mA g^{-1}, 500 mA g^{-1}, 1500 mA g^{-1} as well as 3000 mA g^{-1}. When the current density returned to 100 mA g^{-1}, the reversible capacity remained at 750 mAh g^{-1}, indicating the nanocomposite displayed an excellent electro-chemical performance. One possible explanation for the superior capability and stable cycling performance of the material was that graphene wafer had a large contact surface area with the electrolyte. Moreover, the lithium ions could be adsorbed to the surface of graphene layers physically during the charging and discharging cycles because of the extensive surface area.

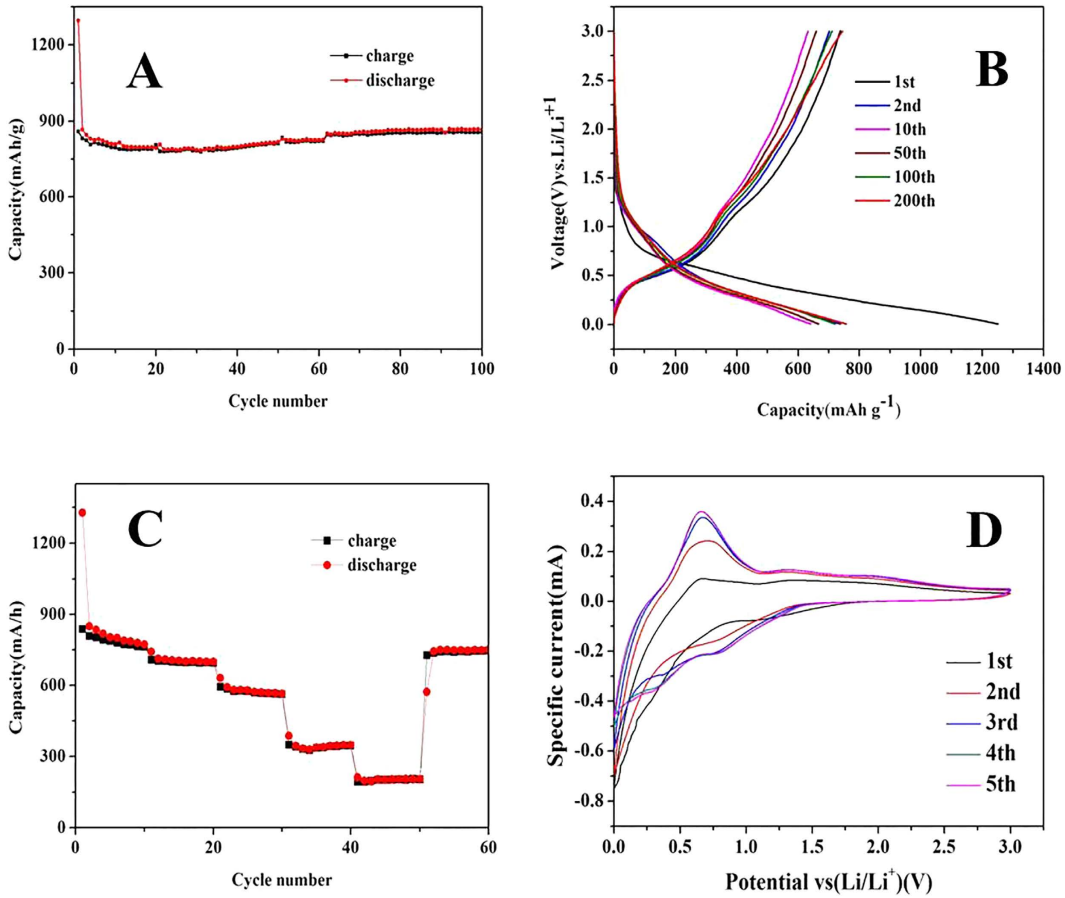

Figure 4. (**A**) Cycling test for the graphene sheet at the current density of 100 mAh g^{-1};(**B**) Discharge/charge profiles (1st, 2nd, 10th, 50th, 100th, 200th cycle) of the as-prepared graphene sheet at the current density of 200 mAh g^{-1} as a LIB electrode. (**C**) Cycle performance of the graphene sheet as a LIB anode at different current densities. (**D**) CV curves of the graphene sheet as a LIB electrode.

The synergistic effect[34,43,44] between SnO_2 nanoparticles and graphene layers as well as the decomposition of electrolyte could contribute to the increase in capacity[45,46]. Another reason for the superior performance of the electrode was the presence of SnO_2 nanoparticles, and the electrical conductivity, and mechanical flexibility of the graphene structure. The uniform distribution of SnO_2 nanoparticles played a vital role in improving the electrochemical properties of LIBs. Since the graphene wafer prepared was porous and elastic, it could accommodate the volume expansion of SnO_2 during charge/discharge cycles. In addition, the porous and interconnected graphene nanostructure could provide an effective conduction path for electron transfer and accommodate the mechanical strain caused by the Li^+ insertion/extraction[41,47].

Figure 4(D) shows the cycle voltammetry curves (CVs) for the first 5 cycles of the SnO_2-GA between 0 and 3 V vs. Li^+/Li at a sweep rate of 0.5 mV s^{-1}. In the first cycle, the electrode was unstable because no binder was used in the batteries and the contact did not reach an ideal state. After the first cycle, the curves were found to be more consistent. It could be seen from the curves that there were four reduction peaks at 1.21 V, 0.82 V, 0.45 V, ~0.2 V, respectively. Along with the formation of Li_2O, the transition from SnO_2 to Sn (eq 1, eq 2) contributed to the pronounced cathodic peaks of 1.21 V and 0.82 V. The peak at 0.45 V could be attributed to the decomposition of the electrolyte and the formation of solid-electrolyte interphase (SEI) on the surface of SnO_2 and GS[2,17,48]. The Li-Sn alloying (eq 3) and the lithium-ion insertion on the GS surface (eq 4) caused a reduction peak at around 0.1 V. There were two oxidation peaks at 0.63 V and 1.32 V which were related to the de-alloying of Li_xSn (eq 3) and the generation of SnO_2[3,6,49]. It is worth noting that the generally considered irreversible reactions (eq1, eq2) became partially reversible reactions because of the ability of the ultra-small size of SnO_2 to decrease the activation energy[2,3,50]. After the second cycle, the nearly overlapping CV curves reflected a superior reversibility of lithium insertion and extraction reactions.

$$SnO_2 + 2Li^+ + 2e^- \leftrightarrow SnO + Li_2O \quad (1)$$

$$SnO + 2Li^+ + 2e^- \leftrightarrow Sn + Li_2O \quad (2)$$

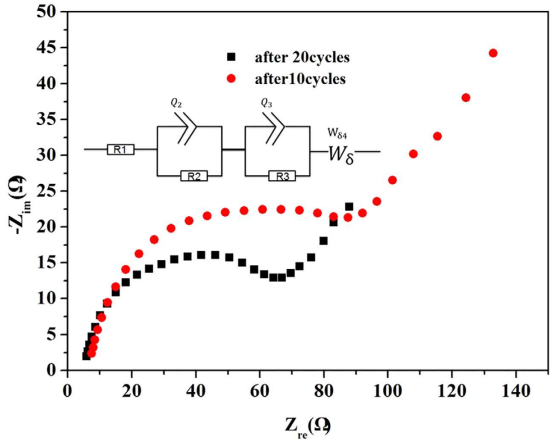

Figure 5. The enlarged high frequency region of the Nyquist plots of SnO_2-rGO.

$$Sn + xLi^+ + xe^- \leftrightarrow LixSn (0 \ll x \ll 4.4) \quad (3)$$

$$C(GN) + xLi^+ + xe^- \leftrightarrow LixC \quad (4)$$

The porous nature of SnO_2/graphene aerogel composite was demonstrated by Brunauer–Emmett-Teller (BET) measurements as shown in Figure S(2). It could be seen in the figure that the N_2 adsorption-desorption isotherms exhibited a typical II hysteresis loop as a relative pressure between 0.45 to 0.96, characteristic of pores with different pore sizes. The nitrogen physisorption measurements traced the change of pore structure and the specific area was calculated to be 168 m^2 g^{-1} while the pore diameter was distributed mainly at approximately 3 nm. These results demonstrated that it is feasible to obtain three dimensional graphene frameworks with solvothermal assembly approach. Moreover, the high porosity provided more surface area for lithium-ions insertion and extraction reactions as well as more room for SnO_2 expansion.

Electrochemical impedance spectroscopy (EIS) measurements were utilized to study the electrode's superior electrochemical performance and the kinetics properties[46]. Figure 5 shows the Nyquist plots of the SnO_2-rGA after 10 cycles and SnO_2-rGA after 200 cycles as well as the equivalent circuit model. It was found that R_2 and R_3 were due to the solid electrolyte interface impedance and to the charge transfer resistance, respectively. Moreover, the liner part of the plot is likely due to the lithium diffusion in the 3D porous network[46,51]. The semicircle diameter of the SnO_2-rGA-20 was smaller than that of SnO_2-rGA-10, implying that the prepared electrodes were stable during charge/discharge cycles[52]. Improved charge transfer and inherent impedance characteristics leading to rate capability enhancement are expected to result from the high electrical conductivity[48].

The TEM images of lithiated and delithiated SnO_2/GA are shown in Fig. 6. Based on the images, it is clear that a SEI layer formed after discharge caused by the decomposition of the electrolyte. The formation of SEI leads to irreversible capacity loss during the initial discharge/charge cycle due to the consumption of Li ions and electrons. Moreover, the SEI layer existed in the delithiated SnO_2/GA and eliminated the volume expansion of SnO_2 nanoparticles, which will lead to an excellent stability, resulting in excellent performance during discharge/charge cycling. Although a SEI layer (Fig. 6(C)) formed on the surface of the graphene layers, it is clear from the images that the SnO_2 nanoparticles did not aggregate and remained dispersed. The strong interaction between SnO_2 nanoparticles and graphene layers together with the three dimensional graphene could effectively eliminate the particles aggregation during cycles. All these features observed and described are expected to lead to a superior cycling performance and stability[52,53]. Comparing Fig. 6(A,B), we concluded that the volume expansion of SnO_2 nanoparticles was eliminated resulted from the homogeneous distribution of SnO_2 nanoparticles on graphene sheets[54]. The robust structure of 3D porous graphene could provide electron transport kinetics for Li ions and buffer the large volume expansion during the long term alloying-dealloying process, prevent the aggregation of SnO_2 nanoparticles and strengthen the contact between the active material and the electrolyte, which would lead to the enhanced cycle performance and rate capacity[49,55,56].

Methods

Synthesis of graphene oxide dispersion. Graphene oxide (GO) dispersion was prepared by a modified Hummers method. Briefly, 3 g of graphite powder, 1.5 g of $NaNO_3$, and 69 ml of H_2SO_4 were mixed in a beaker. 9 g $KMnO_4$ were added into the beaker and stirred. An ice-bath was used to keep the temperature of the mixture to 0 °C. After stirring for 30 minutes, the temperature was raised to 35 °C, while stirring for additional 30 minutes. Subsequently, 138 ml of cold (15 °C) de-ionized water was added slowly. Then, 213 ml of warm (80 °C) water and 15 ml of H_2O_2 were added. The mixture was separated by centrifugation and washed by HCl solution (HCl/H_2O = 1/10) three times. At last, the mixture was dissolved in de-ionized water and dispersed homogeneous by ultrasonic agitation for several hours.

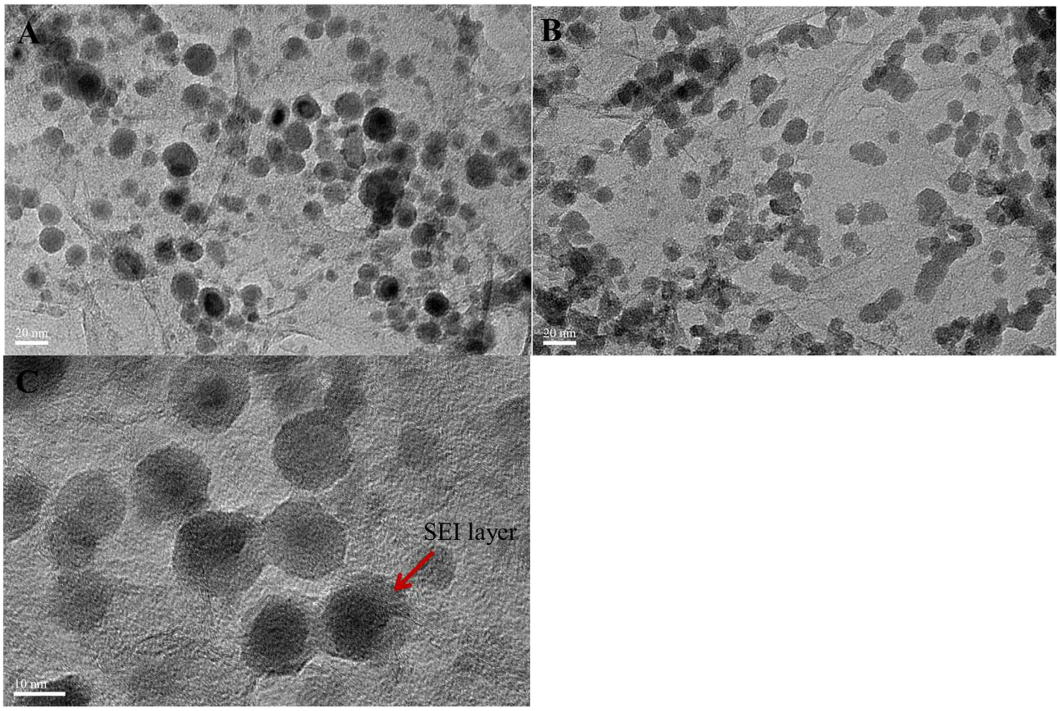

Figure 6. (**A**) TEM image of lithiated SnO_2-GA composite; (**B**) TEM image of delithiated SnO_2-GA composite; (**C**) TEM image of lithiated SnO_2-GA composite.

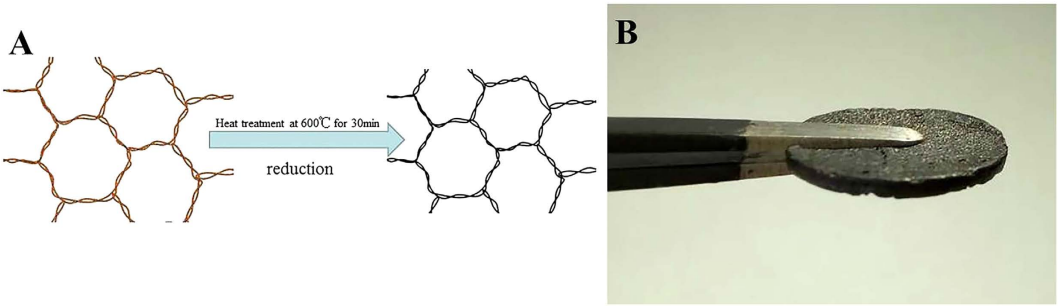

Figure 7. (**A**) Schematic representation of the structure of the GA during annealing treatment; (**B**) Photograph of 3D graphene sheet.

Preparation of SnO_2 nanocrystal. 2.325 g of $SnCl_4{\cdot}5\,H_2O$ was dissolved in 200 ml de-ionized water and then hydrothermally treated at 160 °C for 16 hours. The obtained white precipitate was washed by centrifugation three times and re-dispersed in 200 ml ethanol to form a suspension.

Synthesis of SnO_2/Graphene aerogels. 2.4 ml of SnO_2 dispersion was added drop-wise into 6 ml graphene oxide (2 mg ml^{-1}) so that the mass ratio of graphene oxide and SnO_2 was 1:1. In order to achieve homogeneous dispersion, additional stirring and ultrasonic agitation were carried out for more than 24 consecutive hours. Afterwards, 120 mg of ascorbic acid powder was added into the mixture and stirred for an additional 30 minutes. The dispersion was added into a mold and put into a draught drying cabinet at 75 °C for 4 hours to obtain 3D graphene hydrogels. Subsequently, the monolith was released from the mold and put in de-ionized water for 24 hours, and freeze-dried into graphene aerogel (Fig. 1). Finally, the aerogels was heated at 550 °C for 30 minutes to improve the degree of reduction (Fig. 7(A)).

Electrode Preparation. The graphene aerogels were heated at 650 °C for 30 minutes under nitrogen atmosphere. After being heated, the 3-D graphene sheets (Fig. 7(B)) was used as electrodes without additives or and post-processing.

Material Characterization. The morphology of samples was characterized by transmission electron microscope (JEM-2100F, JEOL, Tokyo, Japan). Field-emission scanning electron microscope (FE-SEM) analysis was performed on JSM-6700F at an acceleration voltage of 10.0 kV. X-ray photoelectron spectroscopic (XPS)

measurements were performed on a Kratos AXIS Ultra DLD spectrometer with a monochromatic AlKa X-ray source. Thermal gravimetic analysis (TGA) was conducted in oxygen atmosphere at a heating rate of 5 °C min^{-1} from 25 °C to 800 °C. X-ray photoelectron spectroscopy (XPS) analysis was conducted using a Kratos AXIS Ultra DLD spectrometer with a monochromatic AlKa X-ray source. Conductivity was measured by a four-point probe method in the van der Pauw configuration with an Accent HL5500 system. N_2 adsorption/desorption isotherms were determined by an Auto sorb IQ instrument. The Brunauer-Emmett-Teller (BET) method was carried out to calculate the surface areas.

References

1. Jiao, Y. *et al.* Fabrication of three-dimensionally interconnected nanoparticle superlattices and their lithium-ion storage properties. *Nat. Commun.* **6,** 6420 (2015).
2. Zhou, X., Wan, L. J. & Guo, Y. G. Binding SnO_2 nanocrystals in nitrogen-doped graphene sheets as anode materials for lithium-ion batteries. *Adv. Mater.* **25,** 2152–2157 (2013).
3. Liu, L., An, M., Yang, P. & Zhang, J. Superior cycle performance and high reversible capacity of SnO_2/graphene composite as an anode material for lithium-ion batteries. *Sci. Rep*. **5,** 9055 (2015).
4. Huang, X., Zeng, Z., Fan, Z., Liu, J. & Zhang, H. Graphene-based electrodes. *Adv. Mater.* **24,** 5979–6004 (2012).
5. Tang, J., Yang, J., Zhou, X., Yao, H. & Zhou, L. A porous graphene/carbon nanowire hybrid with embedded SnO_2 nanocrystals for high performance lithium ion storage. *J. Mater. Chem. A* (2015).
6. Shen, R. *et al.* Synthesis of cambered nano-walls of SnO_2/rGO composites using a recyclable melamine template for lithium-ion batteries. *J. Mater. Chem. A* **3,** 17635–17643 (2015).
7. Gong, C. *et al*. Green synthesis of 3D SnO_2/graphene aerogels and their application in lithium-ion batteries. *RSC Adv*. **5,** 39746–39751 (2015).
8. Han, S., Wu, D., Li, S., Zhang, F. & Feng, X. Porous graphene materials for advanced electrochemical energy storage and conversion devices. *Adv. Mater.* **26,** 849–864 (2014).
9. Qiu, L. *et al.* Mechanically robust, electrically conductive and stimuli-responsive binary network hydrogels enabled by superelastic graphene aerogels. *Adv. Mater.* **26,** 3333–3337 (2014).
10. Wu, Z. S. *et al.* 3D nitrogen-doped graphene aerogel-supported Fe_3O_4 nanoparticles as efficient electrocatalysts for the oxygen reduction reaction. *J. Am. Chem. Soc.* **134,** 9082–9085 (2012).
11. Wang, R. *et al.* Free-standing and binder-free lithium-ion electrodes based on robust layered assembly of graphene and Co_3O_4 nanosheets. *Nanoscale* **5,** 6960–6967 (2013).
12. Worsley, M. A. *et al.* Synthesis of graphene aerogel with high electrical conductivity. *J. Am. Chem. Soc.* **132,** 14067–14069 (2010).
13. Liu, F., Song, S., Xue, D. & Zhang, H. Folded structured graphene paper for high performance electrode materials. *Adv. Mater.* **24,** 1089–1094 (2012).
14. Zhao, D. *et al.* From graphite to porous graphene-like nanosheets for high rate lithium-ion batteries. *Nano Res*. **8,** 2998–3010 (2015).
15. Qin, S., Liu, D., Lei, W. & Chen, Y. Synthesis of an indium oxide nanoparticle embedded graphene three-dimensional architecture for enhanced lithium-ion storage. *J. Mater. Chem. A* **3,** 18238–18243 (2015).
16. Wei, D. Writable electrochemical energy source based on graphene oxide. *Sci. Rep*. **5,** 15173 (2015).
17. Liang, R., Cao, H., Qian, D., Zhang, J. & Qu, M. Designed synthesis of SnO_2-polyaniline-reduced graphene oxide nanocomposites as an anode material for lithium-ion batteries. *J. Mater.Chem.* **21,** 17654 (2011).
18. Su, F.-Y. *et al.* Could graphene construct an effective conducting network in a high-power lithium ion battery? *Nano Eng*. **1,** 429–439 (2012).
19. Hwang, J. Y. *et al.* Direct preparation and processing of graphene/RuO_2 nanocomposite electrodes for high-performance capacitive energy storage. *Nano Eng*. **18,** 57–70 (2015).
20. Zhang, J. *et al.* Ultrafine SnO_2 nanocrystals anchored graphene composites as anode material for lithium-ion batteries. *Mater. Res. Bull.* **68,** 120–125 (2015).
21. He, Y. *et al.* Freestanding three-dimensional graphene/MnO_2 composite networks as ultralight and flexible supercapacitor electrodes. *ACS nano* **7,** 174–182 (2012).
22. Miao, F., Shao, C., Li, X., Wang, K. & Liu, Y. Flexible solid-state supercapacitors based on freestanding nitrogen-doped porous carbon nanofibers derived from electrospun polyacrylonitrile@polyaniline nanofibers. *J. Mater. Chem. A* **4,** 4180–4187 (2016).
23. Nguyen, V. H. & Shim, J.-J. Three-dimensional nickel foam/graphene/NiCo2O4 as high-performance electrodes for supercapacitors. *J. Power Sources* **273,** 110–117 (2015).
24. Chen, H. *et al. In situ* growth of NiCo2S4 nanotube arrays on Ni foam for supercapacitors: Maximizing utilization efficiency at high mass loading to achieve ultrahigh areal pseudocapacitance. *J. Power Sources* **254,** 249–257 (2014).
25. Xie, J. *et al. In situ* TEM characterization of single PbSe/reduced-graphene-oxide nanosheet and the correlation with its electrochemical lithium storage performance. *Nano Eng.* **5,** 122–131 (2014).
26. Su, L. *et al.* CoCO 3 submicrocube/graphene composites with high lithium storage capability. *Nano Eng.* **2,** 276–282 (2013).
27. Dong, Y. *et al.* Dually fixed SnO_2 nanoparticles on graphene nanosheets by polyaniline coating for superior lithium storage. *ACS Appl. Mater. Inter*. **7,** 2444–2451 (2015).
28. Sun, W. & Wang, Y. Graphene-based nanocomposite anodes for lithium-ion batteries. *Nanoscale* **6,** 11528–11552 (2014).
29. Srivastava, M. *et al.* Recent advances in graphene and its metal-oxide hybrid nanostructures for lithium-ion batteries. *Nanoscale* **7,** 4820–4868 (2015).
30. Zhang, L.-S. *et al.* Mono dispersed SnO_2 nanoparticles on both sides of single layer graphene sheets as anode materials in Li-ion batteries. *J. Mater. Chem.* **20,** 5462–5467 (2010).
31. Wu, P. *et al.* Self-assembled graphene-wrapped SnO_2 nanotubes nanohybrid as a high-performance anode material for lithium-ion batteries. *J. Alloy. Compd*. **626,** 234–238 (2015).
32. Fei, L. *et al.* Graphene/Sulfur Hybrid Nanosheets from a Space-Confined "Sauna" Reaction for High-Performance Lithium-Sulfur Batteries. *Adv. Mater.* **27,** 5936–5942 (2015).
33. Mahmood, N., Zhang, C., Yin, H. & Hou, Y. Graphene-based nanocomposites for energy storage and conversion in lithium batteries, supercapacitors and fuel cells. *J. Mater. Chem. A* **2,** 15–32 (2014).
34. Xu, Y. *et al.* Solvated graphene frameworks as high-performance anodes for lithium-ion batteries. *Angew. Chem.* **54,** 5345–5350 (2015).
35. Tang, H. *et al.* Conductive resilient graphene aerogel via magnesiothermic reduction of graphene oxide assemblies. *Nano Res*. **8,** 1710–1717 (2015).
36. Vinayan, B. P. & Ramaprabhu, S. Facile synthesis of SnO_2 nanoparticles dispersed nitrogen doped graphene anode material for ultrahigh capacity lithium ion battery applications. *J. Mater. Chem. A* **1,** 3865 (2013).
37. Zhang, X. *et al.* Mechanically strong and highly conductive graphene aerogel and its use as electrodes for electrochemical power sources. *J. Mater. Chem.* **21,** 6494 (2011).
38. Zhou, G. *et al.* Oxygen bridges between NiO nanosheets and graphene for improvement of lithium storage. *ACS nano* **6,** 3214–3223 (2012).

39. Yang, S., Song, X., Zhang, P., Sun, J. & Gao, L. Self-Assembled α-Fe_2O_3 Mesocrystals/Graphene Nanohybrid for Enhanced Electrochemical Capacitors. *Small* **10,** 2270–2279 (2014).
40. Ye, J. *et al.* Solvent-directed sol-gel assembly of 3-dimensional graphene-tented metal oxides and strong synergistic disparities in lithium storage. *J. Mater. Chem. A* **4,** 4032–4043 (2016).
41. Tian, R. *et al.* The effect of annealing on a 3D SnO_2/graphene foam as an advanced lithium-ion battery anode. *Sci. Rep*. **6,** 19195 (2016).
42. Beguin, F., Presser, V., Balducci, A. & Frackowiak, E. Carbons and electrolytes for advanced supercapacitors. *Adv. Mater.* **26,** 2219–2251, 2283 (2014).
43. Raccichini, R., Varzi, A., Passerini, S. & Scrosati, B. The role of graphene for electrochemical energy storage. *Nat. Mater.* **14,** 271–279 (2015).
44. Tian, Q., Zhang, Z., Yang, L. & Hirano, S.-i. Encapsulation of SnO_2/Sn Nanoparticles into Mesoporous Carbon Nanowires and its Excellent Lithium Storage Properties. *Part. Part. Syst. Char*. **32,** 381–388 (2015).
45. Wei, D. & Kivioja, J. Graphene for energy solutions and its industrialization. *Nanoscale* **5,** 10108–10126 (2013).
46. Li, L., Kovalchuk, A. & Tour, J. M. SnO2-reduced graphene oxide nanoribbons as anodes for lithium ion batteries with enhanced cycling stability. *Nano Res*. **7,** 1319–1326 (2014).
47. Khan, M. *et al.* Graphene based metal and metal oxide nanocomposites: synthesis, properties and their applications. *J. Mater. Chem. A* **3,** 18753–18808 (2015).
48. Yang, T. *et al.* A new approach towards the synthesis of nitrogen-doped graphene/MnO_2 hybrids for ultralong cycle-life lithium ion batteries. *J. Mater. Chem. A* **3,** 6291–6296 (2015).
49. Li, W., Yoon, D., Hwang, J., Chang, W. & Kim, J. One-pot route to synthesize SnO_2-Reduced graphene oxide composites and their enhanced electrochemical performance as anodes in lithium-ion batteries. *J. Power Sources* **293,** 1024–1031 (2015).
50. Wang, R., Xu, C., Sun, J., Gao, L. & Yao, H. Solvothermal-induced 3D macroscopic SnO_2/nitrogen-doped graphene aerogels for high capacity and long-life lithium storage. *ACS Appl. Mater. Inter*. **6,** 3427–3436 (2014).
51. Feng, Y., Feng, N., Wei, Y. & Bai, Y. Preparation and improved electrochemical performance of SiCN–graphene composite derived from poly(silylcarbondiimide) as Li-ion battery anode. *J. Mater. Chem. A* **2,** 4168 (2014).
52. Zhou, X., Yin, Y.-X., Wan, L.-J. & Guo, Y.-G. A robust composite of SnO_2 hollow nanospheres enwrapped by graphene as a high-capacity anode material for lithium-ion batteries. *J. Mater. Chem.* **22,** 17456 (2012).
53. Qin, J. *et al.* Graphene networks anchored with Sn@ Graphene as lithium ion battery anode. *ACS nano* **8,** 1728–1738 (2014).
54. Shen, C. *et al.* Synthesis and electrochemical properties of graphene-SnS_2 nanocomposites for lithium-ion batteries. *J. Solid State Electr*. **16,** 1999–2004 (2011).
55. Li, Y., Zhang, H. & Kang Shen, P. Ultrasmall metal oxide nanoparticles anchored on three-dimensional hierarchical porous gaphene-like networks as anode for high-performance lithium ion batteries. *Nano Eng* **13,** 563–572 (2015).
56. Liang, J., Liu, Y., Guo, L. & Li, L. Facile one-step synthesis of a 3D macroscopic SnO_2–graphene aerogel and its application as a superior anode material for Li-ion batteries. *RSC Adv*. **3,** 11489 (2013).

Acknowledgements

This work is supported by the Natural Science Foundation of China (no. 51373096 and no. 11304198) and CAST Foundation (no. 201233). Instrumental Analysis Center of Shanghai Jiao Tong University and National Engineering Research Center for Nanotechnology are gratefully acknowledged for assisting with relevant analyses.

Author Contributions

Z.h.C. and H.L. designed the research, analysed the data and wrote the paper. R.T., H.n.D., C.m.Z. and J.Z. carried out the electrochemical and physical measurements. Y.p.G., H.M.K., Y.j.C., R.D. and H.z.L. performed the electrochemical measurements and other characterization.

Additional Information

Supplementary information accompanies this paper at http://www.nature.com/srep

Competing financial interests: The authors declare no competing financial interests.

How to cite this article: Chen, Z. *et al.* Three dimensional Graphene aerogels as binder-less, freestanding, elastic and high-performance electrodes for lithium-ion batteries. *Sci. Rep.* **6**, 27365; doi: 10.1038/srep27365 (2016).